Combining orthogonal polarization for elongated target detection with GPR

Maurizio Lualdi and Federico Lombardi

Dipartimento di Ingegneria Civile e Ambientale, Politecnico di Milano, Piazza Leonardo da Vinci 32, 20133 Milan, Italy

E-mail: maurizio.lualdi@polimi.it

Received 14 January 2014, revised 17 May 2014
Accepted for publication 8 July 2014
Published 12 September 2014

1. Introduction

Ground penetrating radar is a practical and productive method for non-destructive diagnosis of shallow subsurface which uses high frequency electromagnetic signals to detect changes in soil characteristics (Daniels 2004, Jol 2009). Due to its high-resolution results the technique has been successfully applied in several engineering and environmental fields, for example cultural heritage (Lualdi and Zanzi 2002, Binda *et al* 2005a, 2011), archaeology (Goodman 1995, Hafez *et al* 2008) and UXO clearance (Lualdi and Zanzi 2005, Acheroy 2007).

Along with this feature, the widespread diffusion of GPR is due to the opportunity of providing a three-dimensional model of the site, in which a number of closely spaced bidimensional profiles a re c onnected i n a p redefined se quence. Al though a faster data collection, 2D profiles could lead to incorrect reconstruction of subsurface features, especially when geometry of the investigated targets is complex.

Three-dimensional acquisitions are more time consuming and expensive than bidimensional ones (Yilmaz 2001) because it is necessary to acquire a dense and regular grid of traces, with a sample spacing sufficient to prevent spatial aliasing problems (Yilmaz 2001, Lualdi *et al* 2003). Fulfilling these constraints guarantees a full reconstruction of the geometry of any targets. Specific problems that need a 3D approach to be solved are, for example, urban infrastructures (Bernstein *et al* 2000), geological features (Grasmueck and Weger 2002, Lualdi and Zanzi 2004, Vanneste *et al* 2008), archaeology (Lualdi *et al* 2006,Lorenzo *et al* 2010, Zhao *et al* 2012), cultural heritage (Binda *et al* 2005b, Binda *et al* 2008) and war remnants detection (Zanzi *et al* 2002).

Common georadar sources and receivers consist of dipole antennas parallel to each other and with a fixed distance between them. The transmitting antenna emits an electromagnetic (EM) wavefield whose electric field is polarized parallel to the long axis of the antenna, here referred to as

the alignment condition or the maximum backscattered condition (Balanis 1982, Daniels 2004) the same distinct directivity exists for the receiver dipole. This highly directional character of the dipole radiation pattern may create problems for the acquisition and interpretation of conventional georadar data. Changes of polarization state of the EM field occur, to some degree, upon reflection and transmission: since the waves are vectorial, features exhibiting directionality can strongly modify the state of an incident field, generating the risk of lowering the visibility of a target or even not being able to image it (Roberts 1994).

Daniels *et al* (2003) and Roberts and Daniels (1996) analyzed the influence of target shapes on the polarization through the evaluation of the scattering width of the target against the observation angle. Radzevicius and Daniels (2000) have focused the analysis on circular cylinders, showing that the backscattered fields may be strongly depolarized depending on: the orientation of the cylinder, the dielectrical properties and the radius of the cylinder compared to the incident wavelength. Lehmann (1996) demonstrated how linearly polarized waves may become circularly polarized depending on the contrasts in EM properties of the host media.

To address these phenomena, various studies examined the possibility of recording data at multiple transmitter–receiver configurations (known as multicomponent GPR) where, compared to the standard perpendicular broadside configuration, one or both antennas were rotated to acquire different components of the electric field.

In their works, Streich and Van der Kruk (2007) and Van der Kruk *et al* (2003) presented a multicomponent imaging algorithm that explicitly corrects for far-field radiation patterns by jointly migrating co-polarized and cross-polarized components; Böniger and Tronicke (2012) present an attribute-based processing to improve target characterization by combining geometrical and physical properties of a dual configuration data.

Lehman *et al* (2000) and Van der Kruk *et al* (2002) are two works that also included a description of the benefits of combining multicomponent data. In Lehman *et al* (2000) co-pole data recorded with antennas oriented in mutually perpendicular directions are combined to obtain a pseudo-scalar wavefield formulation suitable for processing with standard scalar migration. Van der Kruk *et al* (2002) develops an algorithm based on a tensorial description of the scattering matrix, combining co-polarized and cross-polarized measurements. The result is a circularly symmetric resolution function.

Radar polarimetry analysis is another approach that uses the four components of the scattering matrix to extract features of buried targets.

Van Gestel and Stoffa (2001) applied the Alford algorithm on the four scattering elements to extract information about the orientation of buried objects that have angle-dependent reflectivity. The work of Villela and Romo (2013) exploits the invariant properties of the scattering matrix, providing a mathematical formulation to estimate the target azimuth allowing the application of standard processing techniques for scalar fields. Sassen and Everett (2009) employed the largest eigenvalue to compute a coherency-based algorithm. Chen *et al* (2001) used eigenvalues and eigenvectors of the scattering matrix to find the orientation and aspect ratio of UXO-like targets.

We proceed along the results presented by Lehman *et al* (2000) and Villela and Romo (2013), this time providing a methodical demonstration of the effect of directionality on elongated objects, with a focus on target detection. The presented approach is based on the stack of GPR data acquired at mutually orthogonal survey direction, without any constraints on the choice of the first profile orientation. The considered strategy is able to ensure the detection of elongated target regardless of any geometrical and physical issue, even when there is a complete polarization mismatch or adverse settings.

After a mathematic formulation of the addressed issue, the performances of the method are evaluated using densely angular sampled data collected through bipolar GPR equipment over a concrete block in which steel bars, with varying diameters, are buried. Furthermore, a successful application in the field of building inspection of the strategy is illustrated presenting a 3D survey's results.

2. Problem statement

Under the assumption of homogeneous soil (disregarding depolarization and dispersion effects), point heterogeneities in the subsurface can be represented by infinitesimal dipoles with moments parallel and proportional to the incident georadar wavefields (Balanis 1989). In case of elongated objects, the target is approximately a dipole antenna with equal geometrical characteristics.

The scattering matrix formulation, which represents a measure of the target response when illuminated by an arbitrary polarized wave, becomes therefore an index of the depolarization degree of the scattered wavefield. The scattering matrix is defined as:

$$S = \begin{bmatrix} S_{xx} & S_{xy} \\ S_{yx} & S_{yy} \end{bmatrix} \tag{1}$$

where the first subscript of the elements represents the transmitter direction and the second one corresponds to the receiver orientation.

Because of the reciprocity condition, the off-diagonal components are degenerated, so the matrix is symmetric. The scattering characteristics can be obtained through the matrix decomposition: the eigenvectors represent the direction of the two axes of the polarization ellipse, while the eigenvalues quantify the target response when the antenna coordinate axis coincides with those of the target (first eigenvalue) and are at right angles to them (second one). For elongated objects and co-pole configuration, the stronger eigenvalue gives the backscattered field when the longest dimension of the dipole is aligned with the target's one (Radzevicius and Daniels 2000).

A rotation of the matrix in equation (1) is often employed for exploiting the variation of responses associated with an alignment mismatch between sources and scatterers (Chen

et al 2001, Villela and Romo 2013). The rotated system is given by:

$$S^{\varphi} = RSR^{T}, \quad \text{where} \quad R = \begin{bmatrix} \cos\varphi & \sin\varphi \\ -\sin\varphi & \cos\varphi \end{bmatrix} \tag{2}$$

where φ represents the angular deviation from the alignment condition. The terms of the matrix S^{φ} become:

$$\begin{aligned} S^{\varphi}_{xx} &= S_{xx}\cos^2\varphi + S_{yy}\sin^2\varphi + \cos\varphi\sin\varphi\left(S_{xy} + S_{yx}\right) \\ S^{\varphi}_{yy} &= S_{xx}\sin^2\varphi + S_{yy}\cos^2\varphi - \cos\varphi\sin\varphi\left(S_{xy} + S_{yx}\right) \\ S^{\varphi}_{xy} &= S_{xy}\cos^2\varphi - S_{yx}\sin^2\varphi + \cos\varphi\sin\varphi\left(S_{yy} - S_{xx}\right) \\ S^{\varphi}_{yx} &= S_{yx}\cos^2\varphi - S_{xy}\sin^2\varphi - \cos\varphi\sin\varphi\left(S_{yy} - S_{xx}\right) \end{aligned} \tag{3}$$

For conductive cylindrical shape targets, scattering from an obliquely incident wave does not introduce additional components that are not present in the incident field (Balanis 1989).

To show the effect of combining mutually orthogonal, we formulate the problem adding the elements in equation (3) together with those in which the quantity (φ) is substituted with (φ+90°). The superscript indicates the **C**ombination resulted element.

$$\begin{aligned} S^{C}_{xx} &= S^{\varphi}_{xx} + S^{\varphi+90^\circ}_{xx} = S_{xx} + S_{yy} \\ S^{C}_{yy} &= S^{\varphi}_{yy} + S^{\varphi+90^\circ}_{yy} = S_{xx} + S_{yy} \\ S^{C}_{xy} &= S^{\varphi}_{xy} + S^{\varphi+90^\circ}_{xy} = 0 \\ S^{C}_{yx} &= S^{\varphi}_{yx} + S^{\varphi+90^\circ}_{yx} = 0 \end{aligned} \tag{4}$$

The obtained scattering matrix thus becomes:

$$S^{C}(t) = \begin{bmatrix} S_{xx} + S_{yy} & 0 \\ 0 & S_{xx} + S_{yy} \end{bmatrix} \tag{5}$$

The eigenvalues decomposition of the product $\boldsymbol{S^{C}}(\boldsymbol{S^{C}})^{T}$, elements that represent the target backscattered magnitude and are index of the polarization state of the wavefield, leads to:

$$\begin{aligned} \left|\lambda_1^{C}\right|^2 &= \left|S_{xx} + S_{yy}\right|^2 \\ \left|\lambda_2^{C}\right|^2 &= \left|S_{xx} + S_{yy}\right|^2 \end{aligned} \tag{6}$$

The results in equations (5) and (6) lead to some significant considerations:

- The angular dependency in the preferred scattered directions (first elements of the obtained scattering matrix $\boldsymbol{S^{C}}$ in equation (5)) is removed.
- Both the diagonal elements in equation (5) include the two-scattering direction, therefore the collected wavefield will result unaffected from any deviation from the alignment condition, even from a complete polarization mismatch (dipole axis orthogonal to the maximum response configuration). This is evident also considering the magnitude eigenvalue formulation.
- The equality between the two eigenvalues $\lambda_1^{C}$and λ_2^{C} in equation (6) means that the obtained wavefield has a circular footprint with no preferred scattering directions. A rotational invariant scattering matrix has been obtained.

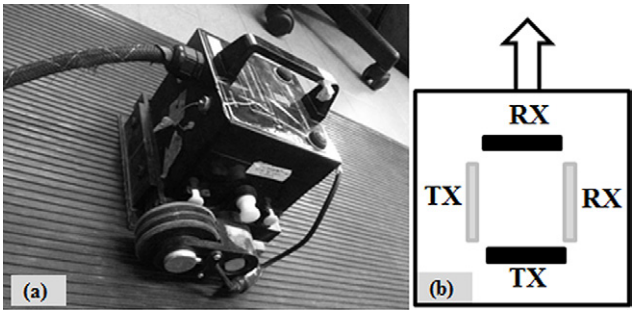

Figure 1. *IDS-Aladdin* georadar equipment. (*a*) Georadar and PSG device. (*b*) Dipoles scheme and geometry.

3. Field example 1: reinforced concrete block

A survey has been performed across three steel rods buried in a concrete block using an *IDS – Aladdin* (Ingegneria dei Sistemi, Italy, figure 1(*a*)) georadar system, which consists of two couples of highly balanced dipole antennas (figure 1(*b*)), with physical length of 6 cm. The central frequency and the bandwidth of the antenna is 2 GHz, with an offset of 6 cm for both couples. This configuration guarantees precise matching between the two *CMP* of the parallel and perpendicular orientation, permitting joint orthogonally polarized scans to be acquired in a single pass.

Three metallic rods with diameter of 16 mm, 10 mm and 6 mm and spaced approximately 30 cm were buried into a concrete block at a depth of 8 cm (figure 2(*a*)). The three diameters represent commonly employed reinforcement dimension for the principal civil engineering structures, from bridges and dams down to housing structures. Inline movements were controlled through *PSG* (Pad System for Georadar, U.S. Patent no. US 7,199,748 B2 of Politecnico di Milano, Italy, Lualdi 2011), and precise angular rotation was achieved through a plate mounted on a protractor (figure 2(*b*)).

The same profile has been acquired in co-pole configuration (dipoles mutually parallel) ten times with an angular sampling of 10° starting with dipoles oriented perpendicular to the survey direction. The selected angular step represents the finer sampling that can provide consistent results considering the accuracy and precision of the described mechanical system.

The dual polarized design of the georadar systems permits simultaneously acquired data from 0° to 180° with a 90° rotation only. The first set of orientation (from 0° to 90°) belongs to one pair of dipoles (black filled in figure 1(*b*), named co-pole perpendicular configuration), while the angles from 100° to 180° to the perpendicular one (grey filled in figure 1(*b*), named co-pole parallel configuration).

Parameters are given in table 1. Single orientation (unstacked) survey results and a sketch of the target to simplify text recalling are shown in figure 3.

Imaging of a linear metallic target is hugely conditioned by alignment mismatch between object and GPR antennas and its influence varies depending on the bar diameter. Globally, visible changes in hyperbola imaging are noticeable at angular variations of approximately 30°.

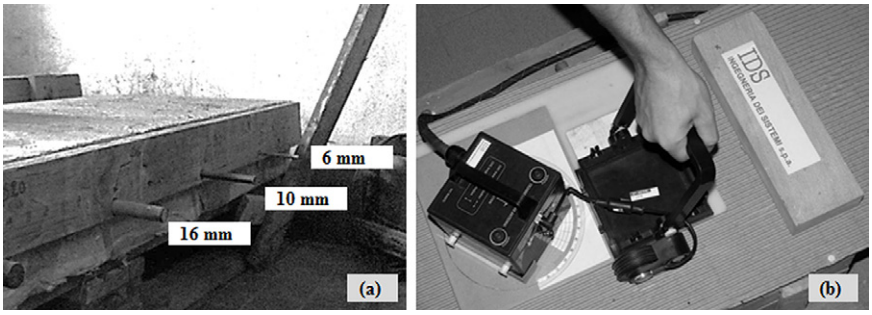

Figure 2. Survey 1: details of the experiments. (*a*) Side view of the concrete block with buried steel bar. (*b*) Georadar antenna and mounted protractor device.

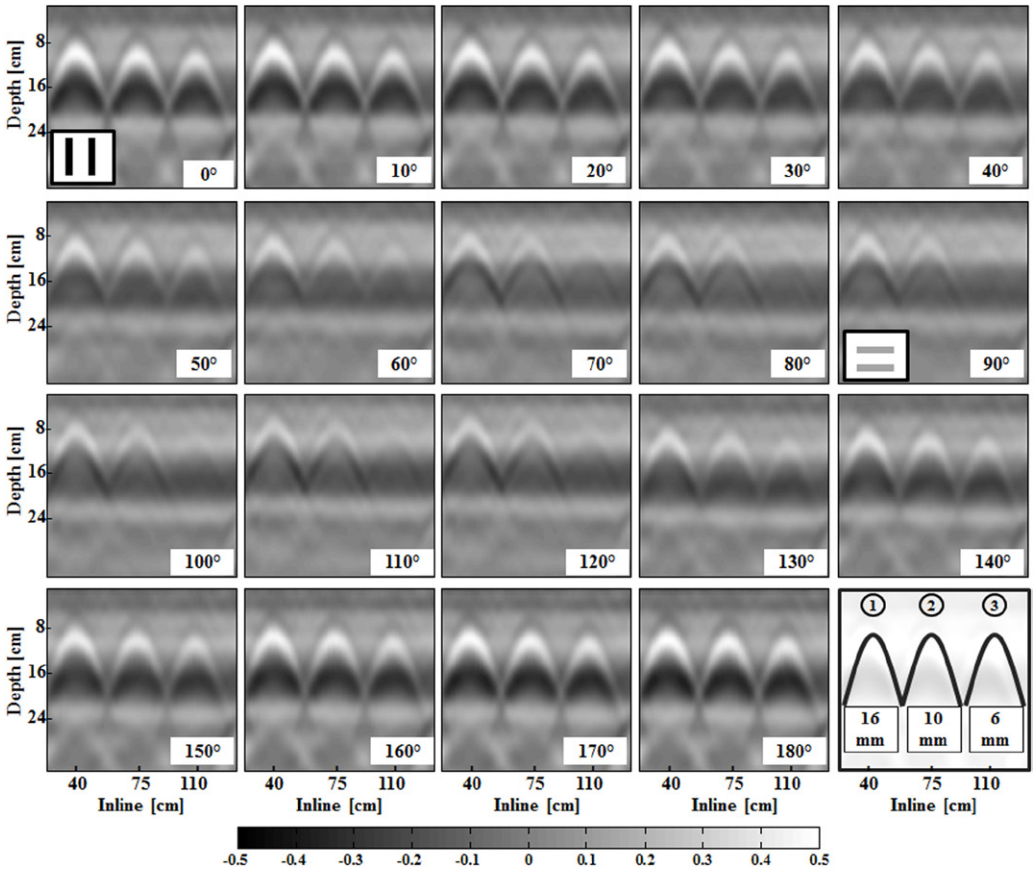

Figure 3. Survey 1: radar profiles of the buried steel bars (for survey geometry and angle definition see text). Single orientation results. All the profiles are plotted using equal amplitude scale and contrast. In the lower corner a sketch of the targets is provided.

Table 1. Concrete block, acquisition parameters.

			Data volume	
Inline sampling(Δx)	Time sampling(Δt)	Time window	X (traces)	T (samples)
0.2 cm controlled by wheel odometer.	0.04 ns	8 ns	380	512

The following trends and considerations can be highlighted:

- The larger rods (particularly target marked 1 in figure 3) are visible at all angles, also when there is a complete polarization mismatch, i.e. approaching 90° orientation (dipoles parallel to the bar); However, their energy is strongly reduced leading to the risk of object missing in case of propagation-related phenomena. Comparing to the optimal alignment (0° and 180° oriented frames) the thickness of the hyperbola is lower and the shape is just outlined.
- The thinner bar (target 3 in figure 3) is extremely affected by deviations from the optimal survey geometry. While its corresponding diffraction hyperbolas are visible up to ~50° and again from 140°, they are significantly attenuated in the range 60° – 130°. When the dipole is approaching orthogonality towards the target (90° rotation),

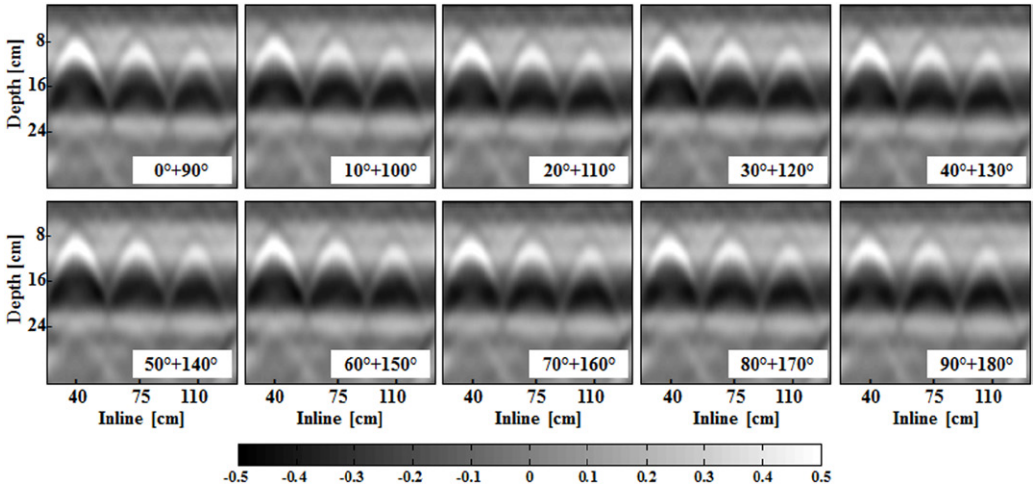

Figure 4. Survey 1: radar profiles of the buried steel bars: combination of mutually orthogonal GPR data results. All the profiles are plotted using equal amplitude scale and contrast.

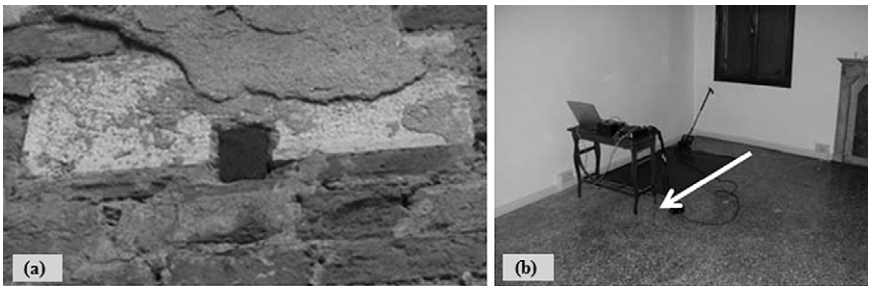

Figure 5. Survey 2: details of the experiments. (*a*) Evidence of a "fiuba" on the façade of a building. (*b*) Acquisition set up: georadar antenna and PSG for the 3D survey. The white arrow represents survey direction and first acquired profile.

the rebar signature vanishes until it becomes not even detectable by the receiver antenna.

- Considering that for a metallic target the maximum response occurs in parallel co-pole configuration with dipoles aligned with the longest axis of the pipe, the orientation that makes the perpendicular co-pole response a maximum also makes the perpendicular a minimum (figure 3, 0° and 90° frames, respectively).

These considerations underline the importance of conducting GPR surveys with two axially rotated measurements to avoid nulls over the thin metallic bar, when using linearly polarized co-pole antennas. Based on this evidence, we develop the approach based on the stack of mutually orthogonal data. The stack is computed after a time calibration (trace peaks shifting) and a trace alignment (cross-correlation technique). The combination results are illustrated in figure 4.

All targets are detected regardless of their diameters and the hyperbola shape is reinstated to a condition nearly close to the most favourable antenna orientation (compared to the 0° or 180° frame in figure 3). We focus the results interpretation on the thinner bar (target 3 in figure 3), which is the target that gains the major advantages from the combination as it suffer the most from misalignment. The first consideration is that the approach overcomes the pitfall of single orientation surveys: all of the combinations lead to a clear target detection. Further on, if one correlates the imaging results of the stacked approach to the optimally aligned orientation of figure 3 (0° or 180° frame), some variations in the hyperbola delineation (mainly due to an enhancement of the bottom of the concrete block) are visible but the hyperbola attributes and characteristics are closely similar. This feature can be observed globally, for the two larger rods (target 2 and 3 in figure 3) as well. Moreover, each of the images in figure 4 provides almost the same information level, demonstrating that combining mutually orthogonal GPR data produces a rotational invariant result and fully recovers the dispersed energy. This performance is explainable considering the symmetric trend of the scattering response from elongated target, in which the maximum of a certain orientation corresponds to the minimum value of its mutually orthogonal one and in the transitory each component compensates the other one.

4. Field example 2: metallic structural elements

A 3D orthogonal dataset was acquired to provide a further demonstration of the previously identified benefits applied to a real situation. The aim of the survey was to detect the so called "fiube", metallic structural elements commonly employed in the Venice area to connect the façade of a building to the floors (figure 5(*a*)).

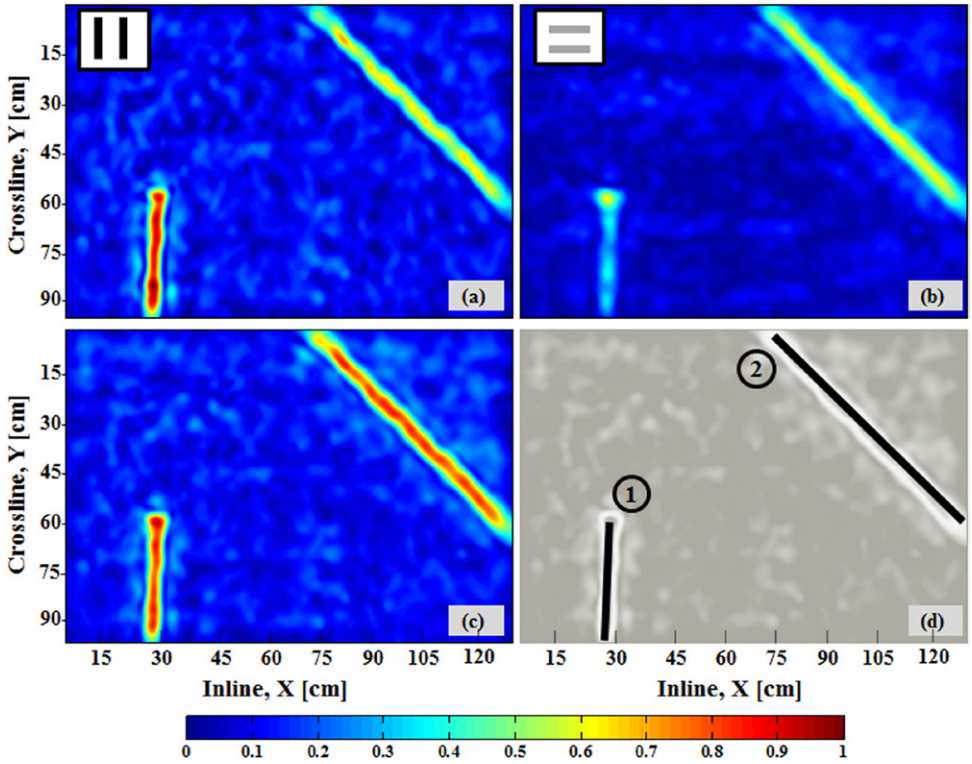

Figure 6. Survey 2: radar depth slice, depth 10 cm. (*a*) Perpendicular configuration. (*b*) Parallel configuration. (*c*) Combination of the two orthogonal volume. (*d*) Schematic layout of the targets. All images are plotted using equal amplitude scale and contrast. In the lower corner a sketch of the targets is provided.

Table 2. Palazzo Pisani, acquisition parameters.

				Data volume		
Inline sampling(Δx)	Crossline sampling(Δy)	Time sampling(Δt)	Time window	Y (profiles)	X (traces)	T (samples)
1 cm controlled by wheel odometer.	1.6 cm controlled by the PSG.	0.04 ns	20 ns	61	140	512

Table 3. Palazzo Pisani, processing steps and details.

Time calibration	Trace alignment	Frequency filtering	Velocity analysis	3D Migration	Data Envelope
Time shift	Correlation window	Zero-phase Butterworth filter. Frequency range: 0.5–3.5 GHz	Synthetic hyperbola fitting on real event. Computed velocity: 16 cm/ns	2D-2step approach (Zanzi and Lualdi 2010)	Hilbert transform

Acquisition was performed on the floor (figure 5(*b*)), the white arrow represents survey direction and starting profile) and parameters are given in table 2.

To obtain a square mesh, data were interpolated to a 0.8 cm step-increment grid. Processing consisted of five steps (Yilmaz 2001), described in table 3.

Two "fiube" are detected (see sketched representation of targets in figure 6(*d*)) and the comparison proves the different sensitivity of the antenna orientation to linear targets. Target oriented perpendicular to the survey direction (target 1 in figure 6(*d*)) is clearly detectable in the co-pole parallel configuration (figure 6(*a*)), while almost invisible in the mutually orthogonal one (co-pole perpendicular, figure 6(*b*)), except for a 3D scattering effect at the end of the bar. Concerning the inclined fiuba (target 2 in figure 6(*d*)), its representation is visible in both configurations with a substantially lower energy response.

The combination of the two orthogonal data volumes (figure 6(*c*)) confirms that the effect of the stack is a compensation for the geometrical misalignment losses. If one compares the energetic level (through the colourbar of figure 6) of the inclined target (target 2) before and after the stack with the other element (target 1 in figure 6(*a*)), that represents the energetic benchmark as it is optimally aligned with the antenna configuration, the demonstration of the amplitude decay recovery is evident. The consequence is a precise reconstruction of targets regardless of their orientation.

5. Discussion and conclusion

An approach that takes into account the polarization characteristics of radar wavefields to guarantee full target detection, overtaking traditional pitfalls in GPR data interpretation has been developed and evaluated. Pitfalls are due to the effect of target directivity features that significantly modify the backscattered wavefield, thus leading to the possibility of corrupted radar results. The presented acquisition and processing technique is based on the combination of mutually orthogonal GPR data, strategy that is proven to be able to remove any angular dependencies turning the expected backscattered elliptical wavefield into a circular one, with no preferred scattering direction.

The method has been first exploited through the evaluation and decomposition of the resulting scattering matrix, which gives evidence to the modifications of the computed eigenvalues of the matrix, elements that define the backscattered magnitude and thus are index of the polarization plane of the reflected wavefield. Two field examples are provided, one bidimensional survey focused on steel rods, that represent probably the most critical target when addressing polarization issues (figure 3), and a 3D application for civil engineering purposes (figure 6). Both the examples demonstrate that combining mutually orthogonal GPR data results in images that do not suffer from misalignment or angular drifts effects, recovering the energy losses and leading to final results that are energetically comparable to the ones that would be obtained under the optimal alignment condition (figure 4 and Figure fc).

These results encouraged the successful application of the multiazimuth technique in the cultural heritage (Lualdi and Lombardi 2013) and archaeological investigations (Lualdi and Lombardi 2014), but remarkable advantages can be gained for mapping and locating underground utilities, although a deeper evaluation of the performances when employing GPR arrays and positioning devices must be carried out (Böniger and Tronicke 2010).

Acknowledgment

Authors are grateful for the support of *IDS* Company for the supply of *Aladdin* georadar equipment.

References

Acheroy M 2007 Mine action status of sensor technology for close-in and remote detection of anti-personnel mines *Near Surf. Geophys.* **5** 43–55

Balanis C A 1982 *Antenna Theory: Analysis and Design* (New York, USA: Wiley & Sons)

Balanis C A 1989 *Advanced Engineering Electromagnetics* (New York, USA: Wiley & Sons)

Bernstein R, Oristaglio M, Miller DE, and Haldorsen J 2000 Imaging radar maps underground objects in 3-D *IEEE Comput. Appl. Power* **13** 20–4

Binda L, Cantini L, Lualdi M, Tedeschi C, Saisi A and Zanzi L 2005b Investigation on structures and materials of the castle of Avio (Trento Italy) *Trans. Built Env.* **2005** 599–610

Binda L, Lualdi M and Saisi A 2008 Investigation strategies for the diagnosis of historic structures on-site tests on avio castle italy and pišece castle slovenia *Can. J. Civil Eng.* **35** 555–66

Binda L, Lualdi M, Saisi A and Zanzi L 2011 Radar investigation as a complementary tool for the diagnosis of historic masonry buildings international *Int. J. Mater. Struct. Integrity* **5** 1–25

Binda L, Zanzi L, Lualdi M and Condoleo P 2005a The use of georadar to assess damage to a masonry bell tower in Cremona Italy *NDT E Int.* **38** 171–9

Böniger U and Tronicke J 2010 On the potential of kinematic GPR surveying using a self-tracking total station evaluating system cross-talk and latency *IEEE Trans. Geosci. Remote Sensors* **48** 3792–8

Böniger U and Tronicke J 2012 Subsurface utility extraction and characterization combining gpr symmetry and polarization attributes *IEEE Trans. Geosci. Remote Sensors* **50** 736–46

Chen CC, Higgins MB, O'Neill K and Detsch R 2001 Ultrawide-bandwidth fully-polarimetric ground penetrating radar classification of subsurface unexploded ordnance *IEEE Trans. Geosci. Remote Sensors* **39** 1221–30

Daniels D J 2004 *Ground Penetrating Radar* (London, UK: IEE)

Daniels J J, Wielopolski L, Radzevicius S and Bookshar J 2003 3D GPR polarization analysis for imaging complex objects *Proc. Symp. on Application of Geophys. to Engineering and Environ. Problems (SAGEEP 2003)* (*San Antonio,USA, 2003*)

Goodman D, Nishimura Y and Rogers J D 1995 GPR time slices in archaeological prospection *Archaeol. Prospect.* **2** 85–9

Grasmueck M and Weger R 2002 3D GPR reveals complex internal structure of pleistocene oolitic sandbar *The Lead. Edge* **21** 634–9

Hafez MA, Atya MA, Hassan AM, Sato M, Wonik T and El-Kenawy AA 2008 Shallow geophysical investigations at the akhmim archaeological site suhag egypt *Appl. Geophys.* **5** 136–43

Jol H M ed 2009 *Ground Penetrating Radar Theory and Applications* (Amsterdam, The Netherlands: Elsevier)

Lehmann F 1996 Fresnel equations for reflection and transmission at boundaries between two conductive media with application to georadar problems *6th Int. Conf. on Ground Penetrating Radar* (*Sendai, Japan, 1996*) pp 555–600

Lehmann F, Boerner D, Holliger K and Green A 2000 Multicomponent georadar data Some important implications for data acquisition and processing *Geophysics* **65** 1542–52

Lorenzo H, Novo A, Rial FI and Solla M 2010 Three-dimensional Ground-penetrating radar strategies over an indoor archaeological site convent of santo domingo (lugo spain) *Archaeol. Prospect.* **17** 213–22

Lualdi M 2011 True 3D Acquisition using GPR over small areas A cost effective solution *Proc. Symp. on Application of Geophys. to Engineering and Environ. Problems* (*Charleston, USA, 2011*) pp 541–50

Lualdi M and Lombardi F 2014 Effects of antenna orientation on 3-D ground penetrating radar surveys an archaeological perspective *Geophys. J. Int.* **196** 818–27

Lualdi M and Lombardi F 2013 Orthogonal polarization approach for three dimensional georadar surveys *NDT E Int.* **60** 87–99

Lualdi M and Zanzi L 2004 2D and 3D experiments to explore the potential benefit of GPR investigations in planning the mining activity of a limestone quarry *Proc. 10th Int. Conf. Ground Penetrating Radar* (*Delft, The Netherlands, 2004*) 613–6

Lualdi M and Zanzi L 2005 Testing a safe acquisition procedure for an effective application of GPR to security operations *Proc. Symp. on Application of Geophys. to Engineering and Environ. Problems* (*Atlanta, USA, 2005*) 613–23

Lualdi M, Binda L and Zanzi L 2003 Acquisition and processing requirements for high quality 3D reconstructions from GPR investigations *Proc. NDT-CE Int. Conf.* (*Berlin, Germany, 2003*)

Lualdi M and Zanzi L 2002 GPR investigations to reconstruct the geometry of the wooden structures in historical buildings *Proc. SPIE* **4758** 63–7

Lualdi M, Zanzi L and Sosio G 2006 A 3D GPR survey methodology for archaeological applications *11th Int. Conf. on Ground Penetrating Radar* (*Columbus, USA, 2006*)
Radzevicius S J and Daniels J J 2000 Ground penetrating radar polarization and scattering from cylinders *J. Appl. Geophys.* **45** 111–25
Roberts R L 1994 Analysis of theoretical modelling of GPR polarization phenomena (*PhD dissertation The Ohio State University*)
Roberts R L and Daniels J J 1996 Analysis of GPR polarization phenomena *J. Environ. Eng. Geophys.* **1** 139–57
Sassen D S and Everett M E 2009 3D polarimetric GPR coherency attributes and fullwaveform inversion of transmission data for characterizing fractured rock *Geophysics* **74** J23–34
Streich R and Van der Kruk J 2007 Accurate Imaging of Multicomponent GPR Data Based on Exact Radiation Patterns *IEEE Trans. Geosci. Remote Sensors* **45** 93–103
Van der Kruk J, Wapenaar C P A, Fokkema J T and Van den Berg P M 2003 Three-dimensional imaging of multicomponent ground penetrating radar data *Geophysics* **68** 1241–54
Van der Kruk J, Zeeman J H and Groenenboom J 2002 Multicomponent imaging of different objects with different strike orientations *Proc. of SPIE* **4758** 150–5
Van Gestel J P and Stoffa P L 2001 Application of Alford rotation to ground-penetrating radar data *Geophysics* **66** 1781–92
Vanneste K, Verbeek K and Petermans T 2008 Pseudo 3D imaging of a slow-slip-rate active normal fault using shallow geophysical methods The Geleen fault in the Belgian Maas River valley *Geophysics* **73** B1–9
Villela A and Romo J M 2013 Invariant properties and rotation transformations of the GPR scattering matrix *J. Appl. Geophys.* **90** 71–81
Yilmaz O 2001 *Seismic Data Analysis* (Tulsa Society of Exploration Geophysicists)
Zanzi L, Lualdi M, Braun H M, Borisch W and Triltzsch G 2002 An ultra-high frequency radar sensor for humanitarian demining tested on different scenarios in 3D imaging mode *Proc. of SPIE* **4758** 240–5
Zanzi L, and Lualdi M 2010 Analysis of approximations and aperture distortion for 3D migration of bistatic radar data with the two-step approach *J Advances in Signal Processing 2010* 192378
Zhao W K, Tian G, Wang B B, Shi Z J and Lin J X 2012 Application of 3D GPR attribute technology in archaeological investigations *Appl. Geophys.* **9** 261–9